Dielectric resonator nanoantennas at visible frequencies

Longfang Zou,[1] Withawat Withayachumnankul,[1] Charan M. Shah,[2] Arnan Mitchell,[2,3] Madhu Bhaskaran,[2] Sharath Sriram,[2] and Christophe Fumeaux[1,*]

[1]*School of Electrical & Electronic Engineering, The University of Adelaide, Adelaide, SA 5005, Australia*
[2]*Functional Materials and Microsystems Research Group, School of Electrical and Computer Engineering, RMIT University, Melbourne, VIC 3001, Australia*
[3]*Centre for Ultrahigh bandwidth Devices for Optical Systems (CUDOS), School of Electrical and Computer Engineering, RMIT University, Melbourne, VIC 3001, Australia*
[*]*cfumeaux@eleceng.adelaide.edu.au*

Abstract: Drawing inspiration from radio-frequency technologies, we propose a realization of nano-scale optical dielectric resonator antennas (DRAs) functioning in their fundamental mode. These DRAs operate via displacement current in a low-loss high-permittivity dielectric, resulting in reduced energy dissipation in the resonators. The designed nonuniform planar DRA array on a metallic plane imparts a sequence of phase shifts across the wavefront to create beam deflection off the direction of specular reflection. The realized array clearly demonstrates beam deflection at 633 nm. Despite the loss introduced by field interaction with the metal substrate, the proposed low-loss resonator concept is a first step towards nanoantennas with enhanced efficiency. The compact planar structure and technologically relevant materials promise monolithic circuit integration of DRAs.

OCIS codes: (230.5750) Resonators; (260.5740) Resonance; (310.6628) Subwavelength structures; (350.4238) Nanophotonics and photonic crystals.

References and links

1. E. N. Grossman, J. E. Sauvageau, and D. G. McDonald, "Lithographic spiral antennas at short wavelengths," Appl. Phys. Lett. **59**, 3225–3227 (1991).
2. I. Wilke, W. Herrmann, and F. Kneubühl, "Integrated nanostrip dipole antennas for coherent 30 THz infrared radiation," Appl. Phys. B **58**, 87–95 (1994).
3. C. Fumeaux, W. Herrmann, F. Kneubühl, and H. Rothuizen, "Nanometer thin-film Ni-NiO-Ni diodes for detection and mixing of 30 THz radiation," Infrared Phys. Technol. **39**, 123–183 (1998).
4. C. Fumeaux, J. Alda, and G. D. Boreman, "Lithographic antennas at visible frequencies," Opt. Lett. **24**, 1629–1631 (1999).
5. M. I. Stockman, "Nanoplasmonics: past, present, and glimpse into future," Opt. Express **19**, 22029–22106 (2011).
6. M. L. Brongersma, "Plasmonics: Engineering optical nanoantennas," Nat. Photonics **2**, 270–272 (2008).
7. P. Bharadwaj, B. Deutsch, and L. Novotny, "Optical antennas," Advances in Optics and Photonics **1**, 438–483 (2009).
8. L. Novotny and N. van Hulst, "Antennas for light," Nat. Photonics **5**, 83–90 (2011).
9. N. Berkovitch, P. Ginzburg, and M. Orenstein, "Nano-plasmonic antennas in the near infrared regime," J. Phys. Condens. Matter **24**, 073202 (2012).

#180556 - $15.00 USD Received 26 Nov 2012; revised 26 Dec 2012; accepted 26 Dec 2012; published 11 Jan 2013

10. M. Danckwerts and L. Novotny, "Optical frequency mixing at coupled gold nanoparticles," Phys. Rev. Lett. **98**, 026104 (2007).
11. F. Tam, G. P. Goodrich, B. R. Johnson, and N. J. Halas, "Plasmonic enhancement of molecular fluorescence," Nano Lett. **7**, 496–501 (2007).
12. Y. Liu, S. Palomba, Y. Park, T. Zentgraf, X. Yin, and X. Zhang, "Compact magnetic antennas for directional excitation of surface plasmons," Nano Lett. **12**, 4853–4858 (2012).
13. J. Li, A. Salandrino, and N. Engheta, "Optical spectrometer at the nanoscale using optical Yagi-Uda nanoantennas," Phys. Rev. B: Condens. Matter **79**, 195104 (2009).
14. T. Kosako, Y. Kadoya, and H. F. Hofmann, "Directional control of light by a nano-optical Yagi–Uda antenna," Nat. Photonics **4**, 312–315 (2010).
15. P. Mühlschlegel, H. J. Eisler, O. J. F. Martin, B. Hecht, and D. W. Pohl, "Resonant optical antennas," Science **308**, 1607–1609 (2005).
16. S. Lal, S. Link, and N. J. Halas, "Nano-optics from sensing to waveguiding," Nat. Photonics **1**, 641–648 (2007).
17. A. Kinkhabwala, Z. Yu, S. Fan, Y. Avlasevich, K. Müllen, and W. E. Moerner, "Large single-molecule fluorescence enhancements produced by a bowtie nanoantenna," Nat. Photonics **3**, 654–657 (2009).
18. S. A. Maier, *Plasmonics: Fundamentals and Applications* (Springer Verlag, 2007).
19. A. Petosa and A. Ittipiboon, "Dielectric resonator antennas: A historical review and the current state of the art," IEEE Antennas Propag. Mag. **52**, 91–116 (2010).
20. S. Long, M. McAllister, and L. Shen, "The resonant cylindrical dielectric cavity antenna," IEEE Trans. Antennas Propag. **31**, 406–412 (1983).
21. Q. Lai, G. Almpanis, C. Fumeaux, H. Benedickter, and R. Vahldieck, "Comparison of the radiation efficiency for the dielectric resonator antenna and the microstrip antenna at Ka band," IEEE Trans. Antennas Propag. **56**, 3589–3592 (2008).
22. P. B. Johnson and R. W. Christy, "Optical constants of the noble metals," Phys. Rev. B: Condens. Matter **6**, 4370–4379 (1972).
23. K. M. Luk and K. W. Leung, *Dielectric Resonator Antennas* (Research Studies Press, Hertfordshire, U.K., 2003).
24. J. Ginn, B. Lail, J. Alda, and G. Boreman, "Planar infrared binary phase reflectarray," Opt. Lett. **33**, 779–781 (2008).
25. D. Dregely, R. Taubert, J. Dorfmüller, R. Vogelgesang, K. Kern, and H. Giessen, "3D optical Yagi-Uda nanoantenna array," Nat. Commun. **2**, 267 (2011).
26. N. Yu, P. Genevet, M. A. Kats, F. Aieta, J. P. Tetienne, F. Capasso, and Z. Gaburro, "Light propagation with phase discontinuities: generalized laws of reflection and refraction," Science **334**, 333–337 (2011).
27. X. Ni, N. K. Emani, A. V. Kildishev, A. Boltasseva, and V. M. Shalaev, "Broadband light bending with plasmonic nanoantennas," Science **335**, 427–427 (2012).
28. J. Huang and J. A. Encinar, *Reflectarray Antenna* (Wiley-IEEE Press, 2007).
29. S. Park, G. Lee, S. H. Song, C. H. Oh, and P. S. Kim, "Resonant coupling of surface plasmons to radiation modes by use of dielectric gratings," Opt. Lett. **28**, 1870–1872 (2003).
30. MicroChem Corporation, "Datasheet for Poly(methyl methacrylate) (PMMA)," .
31. C. A. Balanis, *Antenna Theory: Analysis and Design*, 3rd ed. (Wiley, 2005).
32. A. Alù and N. Engheta, "A Hertzian plasmonic nanodimer as an efficient optical nanoantenna," Phys. Rev. B: Condens. Matter **78**, 195111 (2008).

1. Introduction

Early attempts in developing integrated optical antennas can be traced back to the 1990's with experimental demonstrations of micrometer-scale infrared [1–3] and visible light [4] antennas. Since then, interest in this emerging research field has grown rapidly, with increasing sophistication of designs enabled by advancements in the nanofabrication technology. In the last few years, optical antennas have become a very active field of research in physical optics, both theoretically and experimentally [5]. This has lead to impressive progress in the understanding of resonant optical nanostructures [6–9] with potential for tremendous impact in a multitude of applications including on-chip wireless optical communication, ultrafast computation, and biomolecular sensing. Most current realisations of optical antennas are based on plasmonic effects and achieve a strong field enhancement in a gap between two resonant metallic nanostructures. Among several geometries that have been conceptualized, plasmonic structures such as nano-spheres [10], nano-shells [11], nano-blocks [12], or Yagi-Uda antennas [13, 14] are of particular note.

Characteristic effects associated with surface plasmons can be observed in optical metallic

#180556 - $15.00 USD Received 26 Nov 2012; revised 26 Dec 2012; accepted 26 Dec 2012; published 11 Jan 2013

antennas, which are affected by the intrinsic loss in Drude metals at optical frequencies. As the operation frequency approaches the plasma frequency of the metal, the effective wavelength of the coupled wave becomes shorter, or equivalently, the wavenumber starts to diverge significantly from the light line. As a result, the resonant length of the antenna is shortened [15]. Another consequence of the plasmonic effects in resonant metallic structures at optical frequencies is a subwavelength energy confinement that is highly sensitive to local changes—the principle of a subdiscipline of plasmonic sensing [16, 17]. In the view of potential applications, the plasmonic effects can, however, adversely affect the radiation efficiency of these optical antennas, because the electric field penetrates deeply into the metal where it is subject to high Ohmic loss [18]. This article proposes an unconventional dielectric-on-metal-based approach as a pathway toward the design of physically realisable low-loss optical antennas.

2. Concept and design of dielectric resonator nanoantennas

The proposed structures are inspired by microwave DRAs [19], in the form of metal-backed dielectric blocks operating in resonant fundamental modes. This type of antennas, introduced in the 1980's [20], exploits the principle of "radiation losses" in moderate permittivity dielectric resonators. Commonly found microwave DRAs are constructed from low-loss dielectrics with relative permittivity ranging from 8 to 100, shaped as hemisphere, cylinder, or rectangular parallelepiped. The dielectric resonator is typically mounted on a metal coated substrate, which acts as electrical symmetry plane. Since the resonator is operated at the fundamental mode, it is typically in the order of a half-wavelength in size. A high radiation loss of these DRAs, or equivalently a low Q factor, is the basis of coupling to free-space waves. Antennas formed from such resonators are particularly attractive for high frequency operation, as it has been shown that their efficiency remains high with increasing frequencies [21], in contrast to the rapid efficiency degradation in conventional metallic antennas above 30 GHz. Considering that low-loss high-permittivity dielectric materials are available at optical frequencies, it is feasible to extend the use of DRAs to optical frequencies, as a pathway towards increasing the efficiency of resonant optical antennas.

In the present investigation, the optical DRA is designed to resonate at 633 nm (He-Ne lasers red light, 1.96 eV). As shown in Fig. 1(a), the resonator has a cylindrical shape with a height of 50 nm and a diameter of 162 nm. The dielectric material for the resonator is selected as TiO_2 due to its manufacturability and functionality, offering an anisotropic relative permittivity of 8.29 along the planar axes and 6.71 along the cylindrical axis and an estimated loss tangent lower than 0.01. The substrate is a 390 μm-thick silicon wafer coated with a 200 nm thick silver film. The response of silver at 633 nm is described by its measured relative permittivity of $-16.05 + j0.48$ that fully accommodates the effects of electron oscillations and interband transitions [22]. An isolated DRA on a silver backing was simulated in ANSYS HFSS, employing a radiation boundary condition. Figure 1(b) shows the magnitude and phase on reflection and illustrates that the chosen geometry and materials achieve a sufficiently sharp resonance at approximately 645 nm, with a wide range of phase shifts available at nearby frequencies. Hence, designing resonators with different geometries will tune the resonance frequency and also the phase shift that is imparted to a 633 nm incident beam. Figure 1(c) depicts the electric and magnetic field distributions inside the dielectric of the fundamental $HEM_{11\delta}$ resonant mode, which is characterized by a broadside radiation pattern as shown in Fig. 1(d). This radiation pattern corresponds to a short horizontal equivalent magnetic dipole on a metallic plane [23]. It is noted that, despite the fact that the magnetic field markedly penetrates into the silver layer, the mode in the resonator corresponds qualitatively to the behavior of the fundamental dielectric resonator mode known at microwave frequencies [23].

#180556 - $15.00 USD Received 26 Nov 2012; revised 26 Dec 2012; accepted 26 Dec 2012; published 11 Jan 2013

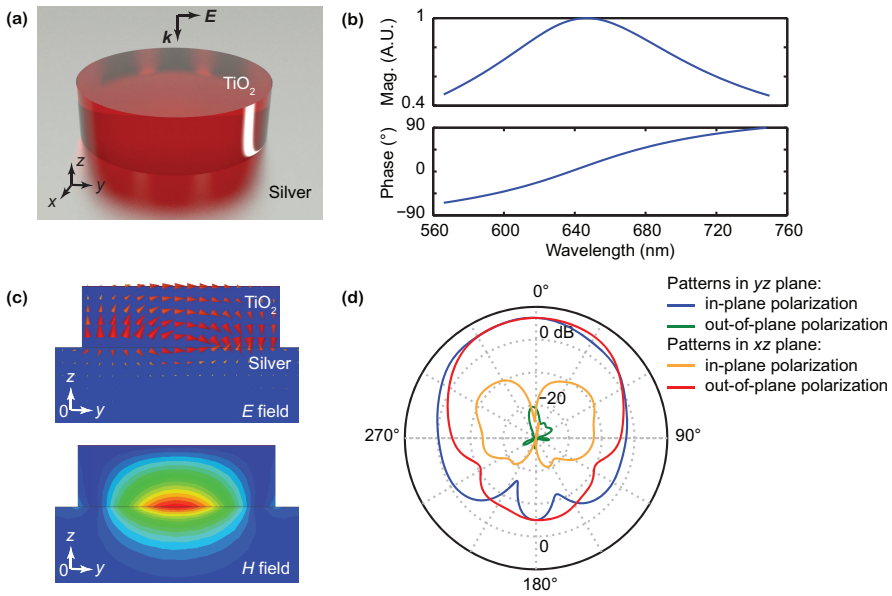

Fig. 1. Single optical DRA and its performance. (a) 3D rendered model of the cylindrical DRA on the silver substrate (not to scale). The cylinder has a diameter of 162 nm and a height of 50 nm. (b) Magnitude and phase of the magnetic field inside the resonator along the *x* axis. (c) Numerically resolved instantaneous field distribution following plane wave excitation. The electric field distribution is represented as vectors, and the magnetic field distribution as colormap. (d) Simulated radiation pattern for in-plane and out-of-plane polarizations. To compute those patterns, the DRA on a finite-size silver plane is excited by a vertical current probe at the periphery of the cylinder. The asymmetry of this source arrangement explains the imperfect symmetry of the patterns.

3. Optical reflectarrays of nano-scale DRAs

The functions and performance of optical DRAs can be analysed in an array configuration with feeding provided by a free-space wave excitation. The array principle has been successfully employed for demonstration of various metallic nanoantennas at optical frequencies [24–27]. It eliminates the need for integrated feeding components, such as sources and guiding channels, and thus minimizes complexity and loss. By combining multiple optical DRAs with different geometries in an array it is possible to observe the coherent (phased) addition of the response of each array element, thus providing information about the phase of the radiated wave that would not be readily accessible with a single optical nanoantenna. As a proof of concept, an array operating in the reflection mode, i.e., a reflectarray [28], can be designed to impart a progressive phase shift to the reflected wave along one axis of the resonator array. The desired phase delay for each element is achieved by varying the diameter of the dielectric resonator to slightly detune it from the resonance. A linear increment in the phase shift imposed to the incident beam upon reflection would result in a predefined angular offset of a deflected beam relative to specular reflection. It should be noted that the principle of operation of the reflectarray differs from that of an optical grating in the sense that the local phase shift is not achieved through a difference in the optical path, but rather through the individual resonance mechanism of antenna elements with sub-wavelength dimensions. As a result, the *angular offset* between the deflected beam and the specular reflection is nearly independent of the angle of incidence and polarisation of the excitation wave.

#180556 - $15.00 USD Received 26 Nov 2012; revised 26 Dec 2012; accepted 26 Dec 2012; published 11 Jan 2013

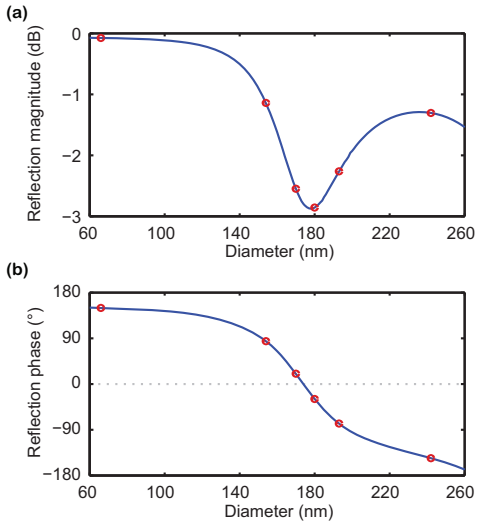

Fig. 2. Numerically resolved magnitude and phase responses of DRAs at 633 nm. The responses vary as a function of the resonators diameter, for a fixed height of 50 nm. The unit cell size is 310×310 nm^2. The simulation employed a periodic boundary condition to mimic the infinite uniform array, and the reference plane is the top surface of the metal plane. The circles indicate the selected cylindrical diameters for the nonuniform array.

Based on the array principle outlined above, a DRA-based optical reflectarray was designed and fabricated. Figure 2 presents the impact of resonator diameter on the magnitude and phase of radiation from individual elements as determined from simulations of infinite and uniform arrays of dielectric resonators with a height of 50 nm. The phase variation obtained from the resonance mechanism can nearly cover the full 360° cycle, whilst the magnitude variation is caused by detuning of the resonator around the resonance. The strongest absorption occurs on resonance and amounts to only -3 dB. It will be shown later that this reflection magnitude variation has a minimal effect on the deflection phase front. By selecting DRAs with a progressive phase increment $\Delta\phi$ of 60° as indicated by the circles in Fig. 2, a sequence of 6 elements can be designed to provide a 360° phase ramp, and this 6-cell linear sub-array can be repeated periodically as shown in Fig. 3(a). The deflection angle θ can be calculated from

$$\sin\theta = \frac{\Delta\phi\lambda_0}{2\pi a}, \tag{1}$$

where λ_0 and a denote the free-space wavelength and unit-cell size, respectively. According to this equation, the reflectarray should exhibit a deflection angle of 19.9° if excited with a normal incident plane wave. This theoretical deflection angle is confirmed by the scattered field of the infinite array of sub-arrays, as shown in Fig. 3(b). The nonuniformity of the reflected wavefront is associated with the grating lobes (also called spatial harmonics or Floquet modes), which will be discussed further in the following. A plasmonic wave can also be observed in the metal layer, since the DRA array acts similarly as a periodic perturbation to match the in-plane momentum of the incident wave to the propagation constant of the surface plasmon polaritons (SPPs) [29].

As described by Eq. 1, the angle of deflection can be predefined by adjusting the progressive phase and distance between the elements. Although in theory the angle of deflection can span $\pm 90°$, The maximal achievable angle of deflection for normal incidence is limited by several practical factors: the beamwidth of the individual element radiation pattern (Fig. 1(d)), the inherent widening of the array factor at larger deflection angles, and the unpredictable mutual

#180556 - $15.00 USD Received 26 Nov 2012; revised 26 Dec 2012; accepted 26 Dec 2012; published 11 Jan 2013

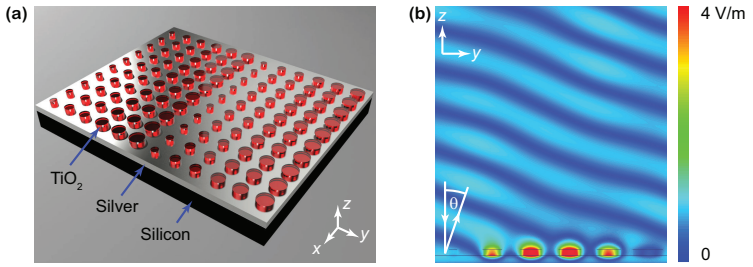

Fig. 3. Geometry of antenna array and scattered fields. (a) Schematic showing a partial view of an antenna array made of 6-cell sub-arrays with DRAs diameters of 66, 154, 170, 180, 193 and 242 nm and a unit-cell size of 310 nm (not to scale). (b) Scattered electric fields of the 6-cell sub-array for the TE-polarized wave, obtained from numerical simulation. The direction of the incident plane wave is perpendicular to the array, and the deflection angle θ equals 19.9° (Media 1).

coupling effects between increasingly dissimilar elements. For reflectarray realizations demonstrated at microwave frequencies, a scanning range of $\pm 40^\circ$ to $\pm 50^\circ$ off broadside can be attained [28].

4. Fabrication of the optical DRA reflectarrays

The linear 6-element sub-array of DRAs was used as a building block for a $\sim 40 \times 40$ μm^2 array containing 126×126 resonator elements. Several arrays were realized by a multi-stage nanofabrication process, incorporating thin film deposition and electron beam lithography (EBL) steps. Figure 4 presents a schematic of the fabrication sequence. Silicon (100) wafers of thickness 390 ± 16 μm and 3" diameter were cleaned in solvents (acetone and isopropyl alcohol) and dried using high purity compressed nitrogen (Fig. 4(a)). A 200 nm thick layer of silver was deposited from a 99.99% pure disc by electron beam evaporation following pumpdown to a base pressure of 1×10^{-7} Torr (Fig. 4(b)). High resolution electron beam resist—poly(methyl methacrylate) or PMMA—was spin-coated onto the silver-coated dies. The electron beam resist coating is a two-step process. First, a layer of EL6 copolymer (PMMA with ~8.5% methacrylic acid, MicroChem Corporation) is spin-coated at 2,750 rpm for 30 s and cured at 150°C for 30 s on a hot plate. Second, a layer of PMMA (MicroChem Corporation) is coated at 2,000 rpm for 30 s and cured at 180°C for 90 s on a hot plate. The thickness of the resulting electron beam resist layer was ~200 nm (Fig. 4(c)) [30]. The PMMA resist layer was patterned by electron beam direct writing in a field emission gun scanning electron microscope (FEG SEM, Nova NanoSEM, FEI Company). The patterning process was controlled by a commercial computer-aided design package (Nanometer Pattern Generation System). Before patterning the actual design, a dose analysis test was performed to obtain the correct dose value at which the PMMA resist should be exposed for optimal pattern transfer. At this dose, the PMMA resist is exposed uniformly without any under or over exposure. The dose analysis was performed by direct write of small and large pattern parameters at various line doses. The resulting patterns were imaged to determine the optimal dose value, which was 0.07 nC·cm^{-1} for the nanoantenna arrays presented in this work. The electron beam patterned PMMA resist was developed using a commercial developer consisting of methyl isobutyl ketone (MIBK) in isopropyl alcohol (IPA) in a 1:3 ratio to obtain high resolution features. The electron beam patterned samples were first rinsed with IPA (to make the resist more hydrophilic) and then dipped in the MIBK:IPA::1:3 developer for 60 s, with the sample constantly agitated during this developing process. A schematic of the resulting structure is shown in Fig. 4(d). The dielectric TiO_2 films of 50 nm thickness were

#180556 - $15.00 USD Received 26 Nov 2012; revised 26 Dec 2012; accepted 26 Dec 2012; published 11 Jan 2013

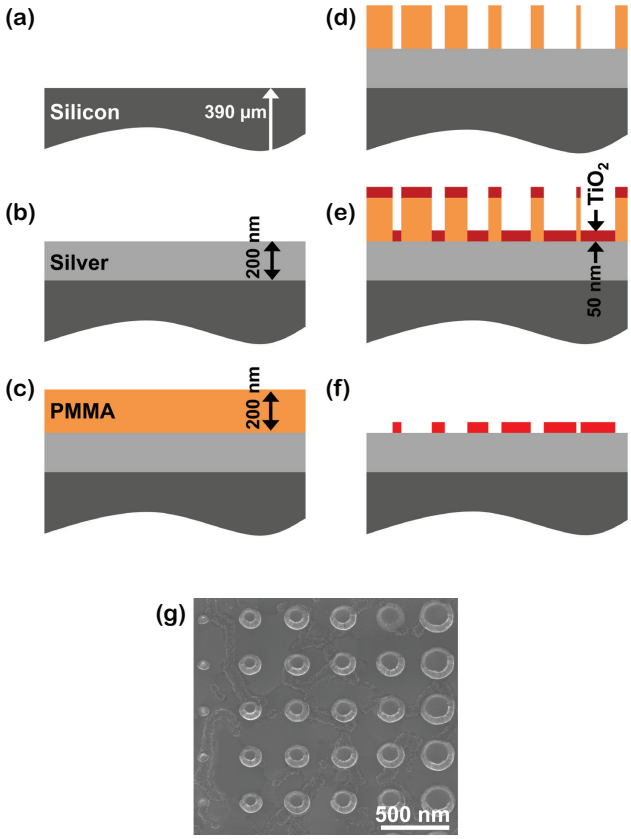

Fig. 4. Schematic of the fabrication sequence for the optical dielectric resonator antenna arrays. (a) Pre-cleaned silicon substrate. (b) 200 nm silver thin film deposited by electron beam evaporation. (c) Electron beam resist (PMMA) spin-coated to attain ∼200 nm thickness. (d) PMMA resist patterned by electron beam direct writing in a field emission gun scanning electron microscope. (e) Dielectric thin film of TiO_2 deposited to a thickness of 50 nm by electron beam evaporation. (f) Finally, the sacrificial PMMA layer is dissolved to attain TiO_2 cylinders which are annealed in vacuum at 600°C for 2 h to attain crystalline material. (g) Scanning electron micrograph revealing a few subarrays.

deposited at room temperature using electron beam evaporation, after attaining a base pressure of 1×10^{-7} Torr (Fig. 4(e)). A lift-off process was then used to obtain the final nanoscale structures by dissolving the sacrificial PMMA layer in acetone with ultrasonic agitation. The resulting nanocylinders of TiO_2 (Fig. 4(f)) were annealed for two hours at 600°C in a vacuum furnace, which was pumped down to a pressure of 1×10^{-5} Torr. The crystallographic analysis of a 50 nm thick uniform TiO_2 layer demonstrated the anatase phase of this film. A small area of the fabricated array shown in Fig. 4(g) illustrates the nonuniform resonator diameters along one axis.

5. Results and discussion

To characterize its reflection characteristics, the antenna array is excited by using a Newport R-31007 linear-polarized red HeNe laser with a wavelength of 633 nm. A microscope lens with a focal length of 16.5 mm tightly focuses the beam to a spot with diameter smaller than 40 μm.

#180556 - $15.00 USD Received 26 Nov 2012; revised 26 Dec 2012; accepted 26 Dec 2012; published 11 Jan 2013

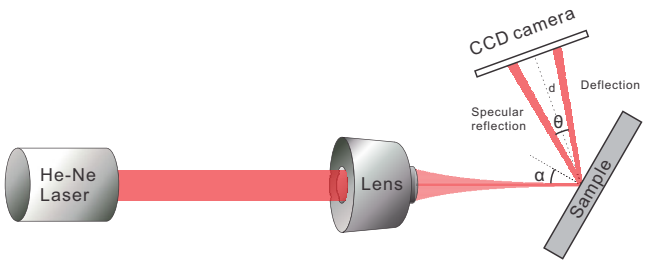

Fig. 5. Experiment Setup. The measurement system comprises a He-Ne CW laser at 633 nm, a microscope objective lens, and a CCD camera. The incident angle α is $\sim 30^\circ$, and the deflection angle θ is $\sim 20^\circ$ from specular direction.

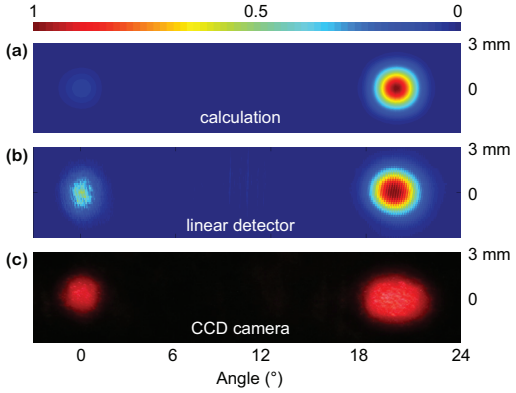

Fig. 6. Beam reflection pattern. The beam reflection patterns obtained from antenna array theory calculation (a), linear camera detector (b), and CCD imaging (c). Angle of 0° denotes the direction of the specular reflection. The theoretical calculation in (a) is obtained by superimposing the phased contributions of the elements in the array (following antenna array theory [31]) with their progressive phase retrieved from the realized resonator diameters (Fig. 4(g) and Fig. 2(b)). The obtained re-radiation angular pattern is subsequently projected on a screen modelled as realized in the experiment.

To measure the specular reflection and the deflection, the incident beam is aligned at an angle α of 30° from normal to the array surface, as illustrated in Fig. 5. A Thorlabs LC100 CCD linear camera is scanned transversally to the direction that bisects the deflection angle θ, and is located 60 mm away from the array surface. The reflection pattern in Fig. 6(a-c) demonstrates a deflection of the main specular beam by the expected 19.9°, while the spatial harmonics are clearly identified. The power ratio of the deflected beam to the zeroth-order spatial harmonic (at the specular angle) determined from the linear camera detector amount to 4.42, demonstrating the expected operation of the reflectarray.

Imperfections evident in the deflected beam are explained by the tolerances of the fabrication, which affect the planar nature of the reflected beam and thus introduce power in the undesired spatial harmonics, as can be estimated from standard antenna array theory [31]. It is worth noting that the small height and area covered by the TiO_2 are not sufficient to explain the deflection through resonant grating diffraction, and therefore, the agreement of the simulation with the experimental results demonstrate the occurrence of a resonance in the individual DRAs. This is further demonstrated by the successful operation of the reflectarray with different sub-array configurations, with measured deflection angles up to 27° (not included in this

#180556 - $15.00 USD Received 26 Nov 2012; revised 26 Dec 2012; accepted 26 Dec 2012; published 11 Jan 2013

report).

The efficiency of the resonant DRAs can be experimentally evaluated from a uniform array of cylindrical resonators with a diameter of 180 nm, a height of 50 nm, and a periodicity of 350 nm. This particular geometry supports the maximum resonance, i.e., zero phase change and strongest absorption. When excited by a Gaussian illumination beam, the array reradiates at an angle corresponding to the specular reflection. Regardless of the incident polarization, both the simulation and measurement reveals that about 35% of the incident power is reflected by the array, normalized to the specular reflection of the bare silver surface. It is anticipated that the missing 65% of the power is absorbed by the array, as plasmonic and dielectric losses. It can be inferred from simulations performed with the TiO_2 dielectric loss set to zero that less than 19% of the incident power be attributed to dissipation in the dielectric resonators, and the remaining 46% is coupled to SPPs. Hence, the dielectric resonator intrinsic efficiency of around 80%, combining the energy of the deflected beam and SPPs, has to be put into perspective of the expected plasmonic antenna efficiency [32]. The plasmonic coupling can potentially be suppressed by replacing the metal plane with a dielectric mirror, whereas in this case a full resonator will have to be considered in the design because of the absence of mirroring plane. On the other hand, dielectric resonators can be optimized to efficiently couple free-space waves to/from SPPs.

6. Conclusion

Optical antennas based on nanometer-scale cylindrical dielectric resonators operating in their fundamental mode have been experimentally demonstrated by using a reflectarray platform to manipulate free-space visible light. The fabricated device comprising an arrangement of TiO_2 cylinders near resonance introduces a progressive phase delay to the wavefront, resulting in a clearly observable beam deflection. The use of low-loss dielectric resonators to concentrate radiation from far-field modes into a sub-wavelength volume opens a new paradigm alternative to purely plasmonic (metallic) antennas. This is the precursor to purely dielectric resonator antennas with minimal energy dissipation. These nano-DRAs provide an additional building block for planar optical components or coupling structures for surface plasmons. Coupled to refinements of manufacture accuracy, advanced designs exploiting these DRAs promise to establish this type of structures in emerging nano-photonics applications, such as short-range optical communications, ultrafast computation, and molecular sensing.

Acknowledgments

W.W., M.B, and S.S. acknowledge Australian Post-Doctoral Fellowships from the Australian Research Council (ARC) through Discovery Projects DP1095151, DP1092717, and DP110100262, respectively. S.S. acknowledges equipment funding from the ARC through LE100100215. C.F. acknowledges the ARC Future Fellowship funding scheme under FT100100585. A.M. time commitment to this project was under the ARC Centre of Excellence program (CE110001018). However this project was not supported with funding from this centre. The authors are grateful to Prof. Derek Abbott and Benjamin S.-Y. Ung, the Adelaide T-ray Facility, for their experimental contributions. The assistance from Sumeet Walia and Geethaka Devendra for processing of TiO_2 and ellipsometry, respectively, is appreciated. Facilities and support from the RMIT Microscopy and Microanalysis Facility is also acknowledged.

#180556 - $15.00 USD Received 26 Nov 2012; revised 26 Dec 2012; accepted 26 Dec 2012; published 11 Jan 2013